ORIGINAL



The isolation and characterization of cellulose nanofibrils from the endocarp of *Cocos nucifera*

Jacob Silliman¹ · Hannes C. Schniepp¹

Received: 6 June 2025 / Accepted: 22 September 2025 / Published online: 18 October 2025 © The Author(s) 2025

Abstract

Coconuts are one of nature's toughest lignocellulosic materials, possessing a fracture toughness on par with dentin and a compressive strength ten times that of bamboo. The coconut's hierarchical structure has been characterized before, except prior studies left out one key aspect, the smallest length scales, approaching the molecular level. Here we exfoliate the hard shell of Cocos nucifera, revealing the true cellular organization and the dimensions of the crystalline cellulose nanofibrils found in the cell walls. After chemical pretreatments, we found entanglement between elongated sclereid cells that was not visible in the untreated coconut shell. This may contribute to the mechanical performance of the endocarp; it also utilizes elongated, high-aspect ratio structural elements at the cellular level, in addition to the nanofibrillar level previously known. Compared to other wood-like materials, the cellulose nanofibrils were shorter and represented a smaller weight fraction. This reduced length and the lower filler-to-matrix ratio could be the optimal lignocellulosic nanostructure for tough biomaterials. These newly discovered unique features explain how the endocarp of Cocos nucifera mechanically outperforms materials consisting of the same molecular components.

Introduction

The endocarp of the coconut exhibits unique mechanical properties that significantly outperform other materials made from the same lignocellulosic biomass. It has a compressive strength of ~ 253 MPa, which is ten times that of bamboo, while only being $\sim 10\%$ denser (Dixon and Gibson 2014; Borrega and Gibson 2015; Flores-Johnson et al. 2018; Lauer et al. 2018). This remarkable strength-to-weight ratio and

Department of Applied Science, School of Computing, Data Sciences & Physics, William & Mary, P.O. Box 8795, Williamsburg, VA 23187, USA



Hannes C. Schniepp schniepp@wm.edu

an elastic modulus of 8–10 GPa (Flores-Johnson et al. 2018; Lauer et al. 2018) make the coconut endocarp a model blueprint for various engineering applications, where lightweight and strong materials are desired. The fracture toughness of $K_{\rm Jc} = 3.2$ MPa m^{1/2} (Gludovatz et al. 2017) is also on par with that of dentin ($K_{\rm Jc} = 3.1$ MPa m^{1/2}), a porous material that absorbs the extreme forces experienced by the teeth, preventing cracks in the enamel (Yan et al. 2008). This high fracture toughness along with an impressive Vicker's hardness of ~500–540 MPa indicates that the coconut endocarp can absorb significant amounts of energy before failing, making it ideal for applications where resistance to crack propagation is critical, such as in protective gear or structural components (Flores-Johnson et al. 2018; Salvini et al. 2018). These mechanical performances are commonly attributed to its outstanding hierarchical structure (Schmier et al. 2020), as shown in Fig. 1. Much like any high-performance material, the structure and makeup at all length scales matter for optimal mechanical properties. Research has been done on the larger length scales (Gludovatz et al.

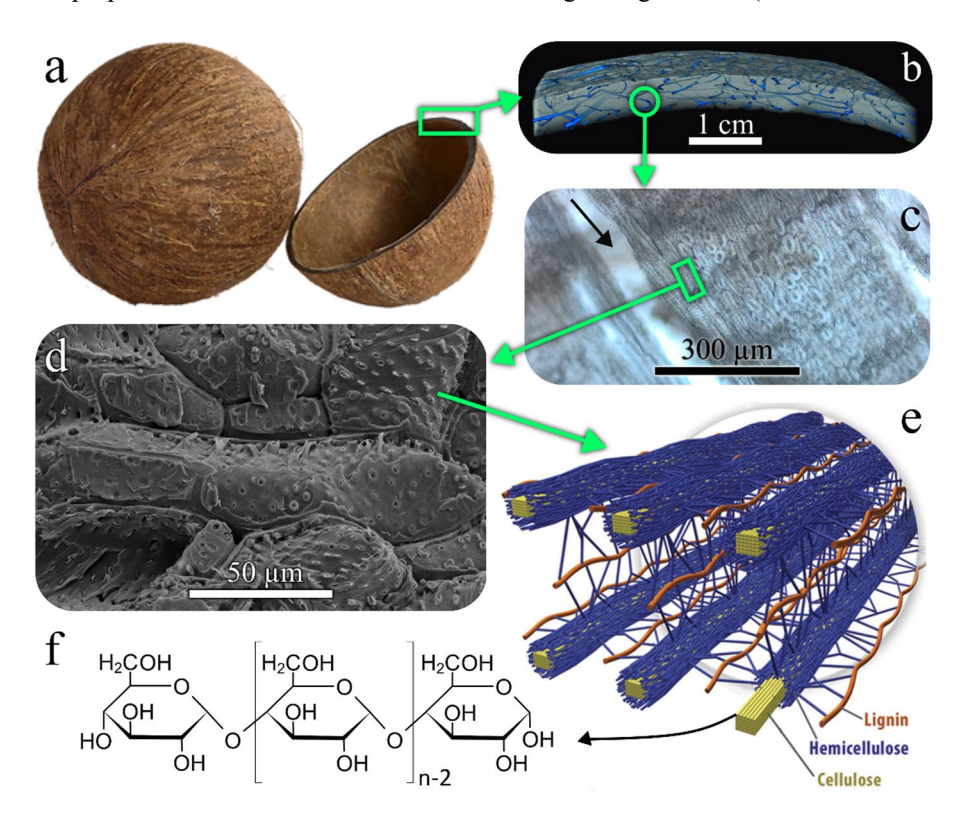


Fig. 1 Hierarchical structure of the endocarp of *Cocos nucifera*: **a** image of the entire coconut endocarp, **b** computed tomography scan of a part of the coconut endocarp, reproduced with permission from: (Schmier et al. 2020), **c** optical microscopy image of one of the vascular channels (black arrow) imaged in **b** surrounded by sclereid cells, **d** field emission scanning electron microscopy image of sclereid cells, **e** schematic of the lignocellulosic structure present in the cell walls, reproduced with permission from: (US Department of Energy Genomic Science program, 2018; US Department of Energy Bioenergy Research Centers, DOE/SC-0191; https://genomicscience.energy.gov), **f** cellulose molecular chain consisting of glucose monomers covalently bonded to each other



2017; Schmier et al. 2020); however, the literature lacks investigations at the smallest length scale, where a material's strength is generally rooted.

At the smallest length scale, all plant-based materials — including wood, bamboo, cotton, hemp, jute — are lignocellulose, a specific arrangement of three components: cellulose, hemicellulose, and lignin. The arrangement and composition of the internal structure at this smallest length scale varies from plant to plant but generally consists of a unique nanofibrillar morphology. This structure is essentially a composite with crystalline cellulose nanofibrils acting as fillers engulfed in a matrix of amorphous hemicellulose and lignin (Fig. 1e). Lignin is the softest of these components, featuring a tensile strength of 50 MPa and an elastic modulus of 3 GPa (Gibson 2012). For hemicellulose, which primarily consists of xylans in the coconut, the mechanical properties are somewhat less clear. While the modulus of xylans is known to be around 7 GPa (Scheller and Ulvskov 2010), their tensile strength is not known. Cellulose is what provides most of the strength in all lignocellulosic biomass. Molecular dynamics simulations have suggested that cellulose crystals have a tensile strength of around 7.5 GPa, about 5 times the strength of steel, and a modulus of 140 GPa (Tashiro and Kobayashi 1991; Eichhorn et al. 2000; Jakob et al. 2022). The alignment and orientation of these cellulose nanofibrils, as well as their degree of crystallinity within a material, can significantly affect the material's mechanical properties. Therefore, an in-depth characterization of these nanofibrillar fillers would be very beneficial in establishing the material's structure-property relationship at the nanoscale, which has previously been assessed via computer modeling (Mazumder and Zhang 2023). An assessment of these fibrils' dimensions, as well as the biomass percentage in relation to hemicellulose and lignin, is still lacking and is key for the development of fully comprehensive computer models. These models can then be used to inform new engineered materials, improving upon things such as bulletproof helmets.

Experimental characterization of individual cellulose nanofibrils requires the decomposition of the coconut endocarp into its constituents. Many other sources for lignocellulosic biomass have already been decomposed into nanofibrils via exfoliation, such as cotton fiber, bamboo, and hemp (Yi et al. 2020). These materials are well-studied for their mechanical and structural properties, which have led to numerous applications in textiles, composites, and biomaterials. However, the endocarp of the coconut has been overlooked, and its exfoliation has not previously been reported. Therefore, a reliable method of exfoliation for the coconut is needed, which in turn can be used as a means of obtaining sustainably sourced lignocellulose.

The use of lignocellulosic biomass waste as a replacement for synthetic fibers and plastics can substantially minimize our environmental impact. The endocarp of a coconut is one of the most abundant forms of lignocellulosic biomass waste, found in over 90 countries with a global production amassing 62.5 million tons per year (Azeta et al. 2021). This large volume highlights not only the widespread cultivation of coconuts but also the potential for utilizing what is currently agricultural waste. As opposed to cutting down trees and further harming the environment, coconut endocarps provide an ecologically sustainable source of lignocellulose. This is particularly important in the context of global deforestation and the need for sustainable resource management. The utilization of coconut shells promotes a circular economy by maximizing resource efficiency and minimizing waste in coconut processing.



Experimental

Materials

Cocos nucifera fruits from the Dominican Republic were purchased at a local grocery store. The endocarps were extracted and thoroughly cleaned and sanded to obtain the final raw shell material. 2,2,6,6-Tetramethylpiperidine 1-oxyl (TEMPO), sodium bromide, sodium hydroxide, a 15% sodium hypochlorite solution, and other chemicals were of laboratory grade (Thermo Scientific Chemicals, US) and used without any further purification.

Exfoliation of Cocos nucifera

Chemical pretreatment

To examine the base cellulose units comprising the endocarp, it first needs to undergo a chemical pretreatment. Therefore, the endocarp was shaved into smaller pieces using a lathe and then submerged in a solution of 2:1 toluene:ethanol. This treatment was done for 120 min, stirred constantly at 500 RPM, then rinsed with deionized (DI) water and vacuum filtered. This dewaxing process was completed thrice to remove all impurities, leaving behind the lignocellulosic material. The material was vacuum dried at room temperature and then 1 g of it was placed into a beaker with 40 mL of water, 0.4 g of sodium chlorite, and 40 μL of acetic acid at 80 °C. After an hour, the respective amounts of sodium chlorite and acetic acid were added again until 4 h had passed (Abe and Yano 2009; Hubbell and Ragauskas 2010). After this delignification, effectively removing most of the lignin, the solution was vacuum filtered and rinsed with DI water, then left to vacuum dry at room temperature. The next step was to remove hemicellulose through an alkaline treatment with potassium hydroxide. The endocarp pulp was added to a beaker with 40 mL of 4 wt% potassium hydroxide solution at 90 °C. This was left for 2 h, then vacuum filtered and vacuum dried at room temperature (Abe and Yano 2009; Modenbach and Nokes 2014). The acidified sodium chlorite delignification method was repeated followed by the alkaline potassium hydroxide treatment to ensure all lignin and hemicellulose were removed.

TEMPO oxidation

TEMPO oxidation was then used to further individualize the remaining cellulose pulp. This oxidation process targets a primary hydroxyl group in the C6 carbon position of the chained glucose monomers that constitute cellulose (de Nooy et al. 1995). It turns this hydroxyl group into a carboxyl group, introducing a negative charge and more repulsion between individual cellulose nanofibrils. 1 g of chemically pretreated pulp was placed into a beaker of 100 mL of DI water along with 0.2 g of sodium bromide and 0.02 g of TEMPO. This was stirred at room temperature for 30 min to allow for dissolution (da Silva Perez et al. 2003; Habibi et al. 2006; Isogai et al. 2010). After this, 2 mL of 15 wt% sodium hypochlorite was added slowly to maintain a pH of 10.5. Once the sodium hypochlorite was used, sodium hydroxide



was added to maintain a solution pH of 10.5 for 120 min (Besbes et al. 2011; Kaffashsaie et al. 2021). After this time, 5 mL of ethanol was added to stop the reaction, and the solution was stirred for another 20 min (Saito and Isogai 2004; Isogai et al. 2011; Ma et al. 2012; Fan et al. 2021). The pulp was subsequently vacuum filtered and then tip-sonicated for 80 min to separate the individual nanofibrils. Centrifugation at 6,000 RPM was done for 30 min, and then the supernatant was separated and analyzed through amplitude-modulation atomic force microscopy (AM-AFM).

Tip sonication

Tip sonication, using the Cole-Parmer CPX750 Ultrasonic Homogenizer (750 W, 20 kHz, 40% amplitude), was employed to mechanically exfoliate the solution of TEMPO-oxidized cellulose. This was done in an ice bath with a cutoff temperature of 50 °C to ensure no degradation of the cellulose due to heat. Ultrasonic pulses of 10 s followed by a 10-second pause were used for 80 min to analyze the level of exfoliation, and 160 min to completely exfoliate the cellulose into a solution of individualized nanofibrils.

Characterization of cellulose nanofibrils

Crystallinity index

The crystallinity index (crystalline fraction) of cellulose was calculated from X-ray diffraction using the Segal method, which compares the intensity of the major crystalline cellulose peak to that of the broad amorphous cellulose background (Segal et al. 1959; Popescu et al. 2008; French and Santiago Cintrón 2013).

Crystal width

An Empyrean PANalytical Series 2 X-ray diffractometer (Cu K_{α} radiation, λ =1.54 Å) was used to perform powder diffraction measurements on a TEMPO-oxidized cellulose nanofibril sample obtained from chemically pretreated coconut endocarp. The sample was pressed into a disk shape and scanned within a 2θ range of 5° to 60° over 6 h.

The substrate for this sample was a silicon wafer with a naturally formed layer of surface oxide. Due to the penetrative nature of the XRD, a background from this substrate can be seen in the cellulose powder scans, giving the diffractogram a slight tilt. To remove this background, the bare substrate was scanned using the same parameters and fit with a basis spline interpolation, which was then subtracted from the cellulose diffractogram. To determine the width of the cellulose nanofibrils, the Debye–Scherrer method was carried out on the (200) peak using a shape factor of K=0.9 (Elazzouzi-Hafraoui et al. 2007; Daicho et al. 2018). Gaussian fits were applied to all diffractogram peaks and a Levenberg-Marquardt algorithm iterated until the total sum of all peaks converged with the diffractogram.



Visualization of cellulose nanofibrils

Atomic force microscopy

100 μ L of the aqueous TEMPO-oxidized coconut cellulose nanofibril (TOCCNF) solution was deposited onto a freshly cleaved piece of mica through spin coating (Laurell WS-400Bz-6NPP) at 2,000 RPM for 2 min (Perera et al. 2023; Silliman et al. 2024). Amplitude-modulation non-contact atomic force microscopy with the NTEGRA Prima Scanning Probe Laboratory (NT-MDT, Zelenograd, Russia) was used to visualize these TOCCNFs. MikroMasch HQ: NSC15/Al BS AFM tips (radius of curvature $r\approx 8$ nm, resonance frequency $f\approx 325$ kHz, and spring constant $k\approx 40$ Nm⁻¹) were used in these scans. Gwyddion software was used to flatten and analyze the AFM topography images (http://gwyddion.net/). For scan sizes>1 μ m×1 μ m, the piezo scanners were operated in closed-loop mode in lateral directions to compensate for the effects of piezo non-linearity and creep. For smaller scan sizes, the piezo scanner was operated in open-loop mode to eliminate noise introduced by the position sensors. To avoid the effects of piezo creep in open-loop mode, positional scanner adjustments were done cautiously and slowly.

Field emission scanning electron microscopy

Shavings of the endocarp were analyzed using a Hitachi S-4700 field emission scanning electron microscope (FESEM) running at an acceleration voltage of 8 kV and a working distance of 8 mm. The samples were attached to an aluminum SEM holder with carbon tape, and sputter-coated (Anatech LTD, Hummer 6.2) with a 3 nm layer of gold/palladium. The goal was to observe the effects of the chemical pretreatments on the surface of the shavings by comparing them to raw shavings that did not undergo chemical pretreatment.

Results and discussion

Exfoliation of Cocos nucifera and characterization of cellulose nanofibrils.

Coconut endocarp shavings were first subjected to delignification (acidified NaClO₂) and alkaline (KOH) pretreatments that have been commonly used in lignocellulosic materials to remove lignin and hemi-cellulose, respectively (Abe and Yano 2009; Hubbell and Ragauskas 2010; Modenbach and Nokes 2014; Zhang et al. 2018). The field-emission scanning electron micrographs (FE-SEM) in Fig. 2 visualize the effects of this treatment. When comparing the untreated (Fig. 2a, b) and the treated (Fig. 2c, d) coconut chips, we can see some major differences. The untreated chip has a thick film coating the sclereid cells with bumpy features evenly dispersed throughout the film, while the treated chip has no film, and the cellulosic structure of the cells is visible. Apparently, the components that the chemical pretreatments targeted, lignin and hemicellulose, create a relatively homogeneous, dense material that obscures the finer details of the underlying cell structure. This makes it more difficult to dis-



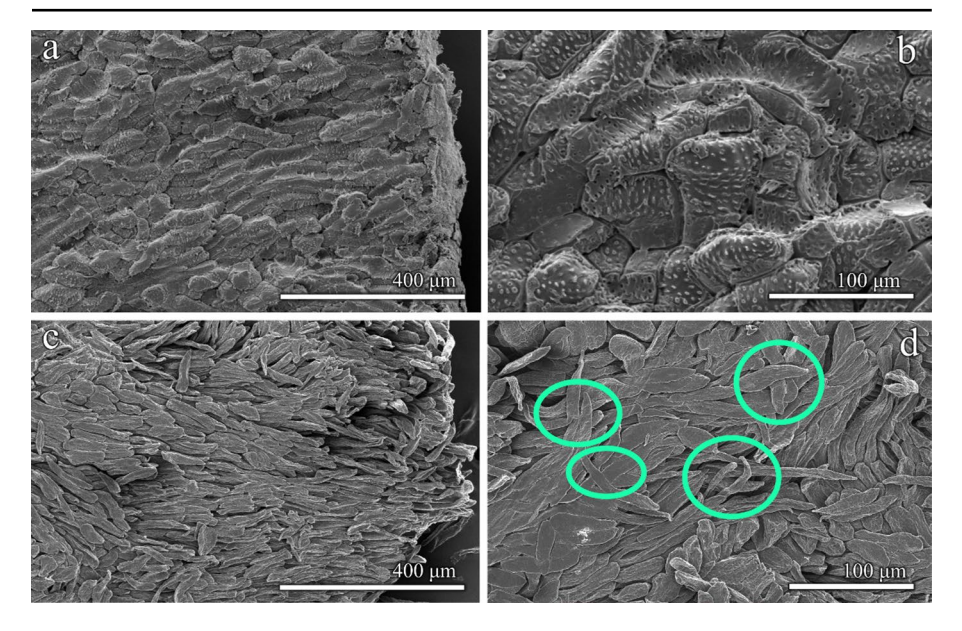


Fig. 2 a Non-treated *Cocos nucifera* endocarp chip, **b** close-up of non-treated sclereid cells, **c** chemically pre-treated *Cocos nucifera* endocarp chip, **d** close-up of chemically pre-treated sclereid cells (green ovals highlighting cell entanglement)

cern the individual cells and their arrangement within the material. Lignin had been suggested to be the primary material in the bumpy "bordered pits" (Schmier et al. 2020) seen coating the sclereid cells in Fig. 2b. With the removal of the bordered pits through the delignification portion of the chemical pretreatment, the surfaces of the cells can be investigated more closely (see Fig. 2c, d).

The enhanced clarity of these cells revealed a clearer view of the organization at this hierarchical level; cells can be seen entangled with one another in a weaving manner (highlighted by green ovals in Fig. 2d) and spanning longer distances than previously visible. Some cells have a "tail" as well as a larger circular "head" seen in Fig. 2d that was not apparent in Fig. 2a, b. These sclereid cells appeared to be ovular in the untreated coconut; however, after treatment, we can see that these structures were previously masked by the film of lignin and hemicellulose. These structures allow the cells to wrap around one another and form this tightly packed woven cell structure (circled in Fig. 2d). The main function of these sclereid cells is mechanical support, and this newly identified entangled structure may provide a better explanation for the outstanding performance of the coconut endocarp than the previous model, which assumed an array of ovular cells. Our evidence revealed that the sclereids are significantly elongated, featuring multiple instances of cells with ~90° orientation, overlapping and passing under 0° oriented cells, forming this entangled/woven microstructure. Hence, the coconut endocarp is essentially a material where elongated, high-aspect ratio structural elements play an important role at two separate length scales: the entangled sclereid cells form a pseudo-fibrous weave at the 10-100 µm length scale, and their cell walls are comprised of crystalline cellulose fibrils 100's of nanometers long, engulfed in lignin and hemicellulose.



All bio-sourced cellulose contains crystalline and amorphous regions. In crystalline cellulose, the structure is very ordered, and there are consistently placed hydrogen bonds between the chains of cellulose (see Fig. 1f), providing strength. Amorphous cellulose, on the other hand, lacks an ordered H-bond network, so that cellulose chains can separate from each other and twist around others randomly. To investigate this aspect specifically for the endocarp, we imaged the TEMPO-oxidized coconut cellulose nanofibrils (TOCCNFs) with atomic force microscopy (AFM, Fig. 3). An overview image of a group of TOCCNFs after tip sonication for 40 min is shown in Fig. 3a. A higher magnification of this sample is shown in Fig. 3b, revealing the two types of cellulose. One type is taller, (white/yellow in the AFM image) consisting of relatively long and straight fibrils seen in the topography maps, indicating flexural rigidity. The second type is less tall (orange/red in the AFM image) and forms a more network-like structure in the background. The shape and size of the first type is in line with literature reports of crystalline cellulose (see green arrow in Fig. 3b); accordingly, they appear straight and stiff, and they are clearly individualized. The second type consists of the non-crystalline cellulose present in the sample (see white arrow in Fig. 3b).

After 80 min of tip sonication, the crystalline cellulose is still present (see Fig. 3c, d). The non-crystalline amorphous component, resembling a fibrous network in the background, is no longer present (see Fig. 3d), suggesting it was unable to withstand extended tip sonication. There is some material in the background of Fig. 3d, appearing as an orange/red globular material splotched throughout the topography map. Most likely, this is debris from the amorphous cellulose broken up during the extended sonication. Tip sonication time has a large effect on how individualized the TOCCNFs are. 40 min at 40% amplitude breaks up the cellulose into smaller groups of fibrils but does not separate them from one another (Fig. 3a, b). During extended tip sonication, the amorphous cellulose that was holding the crystalline fibrils together in the first 40 min is pulverized into smaller chunks, thereby allowing the intact crystalline cellulose to be individualized and dispersed evenly throughout the aqueous solution. 80 min at 40% amplitude was found to be the optimal time for exfoliation into a solution of homogeneous individual TOCCNFs (Fig. 3c).

Length profiles were collected in order to assess the length of the crystalline cellulose nanofibrils. We took 102 measurements of these nanofibrils from end to end, ignoring any bends or kinks in the fibrils. We calculated the number average \pm standard deviation and length-weighted average. The latter was used due to the skewed nature of the distribution (Fig. 3e), similar to what was reported in the literature for wood (Douglas fir) cellulose nanofibrils (Shinoda et al. 2012). The lengths of the cellulose nanofibrils from the coconut endocarp, 155 ± 89 nm, are much shorter than those of the wood, 414 ± 262 nm (Shinoda et al. 2012). This could be due to the curvature of the coconut endocarp, while wood is grown in a straighter and longer manner. The shorter nanofibrils could contribute to the increase in toughness relative to traditional woods, while maintaining a similar density (Dixon and Gibson 2014; Borrega and Gibson 2015). The shorter lengths potentially allow for a less brittle material leading to a high fracture toughness and strain-at-break (Flores-Johnson et al. 2018).

To assess the width of individual TOCCNFs, AFM scan sizes of 600 × 600 nm were used to get a more accurate profile (Fig. 3d, and magnified region of interest in



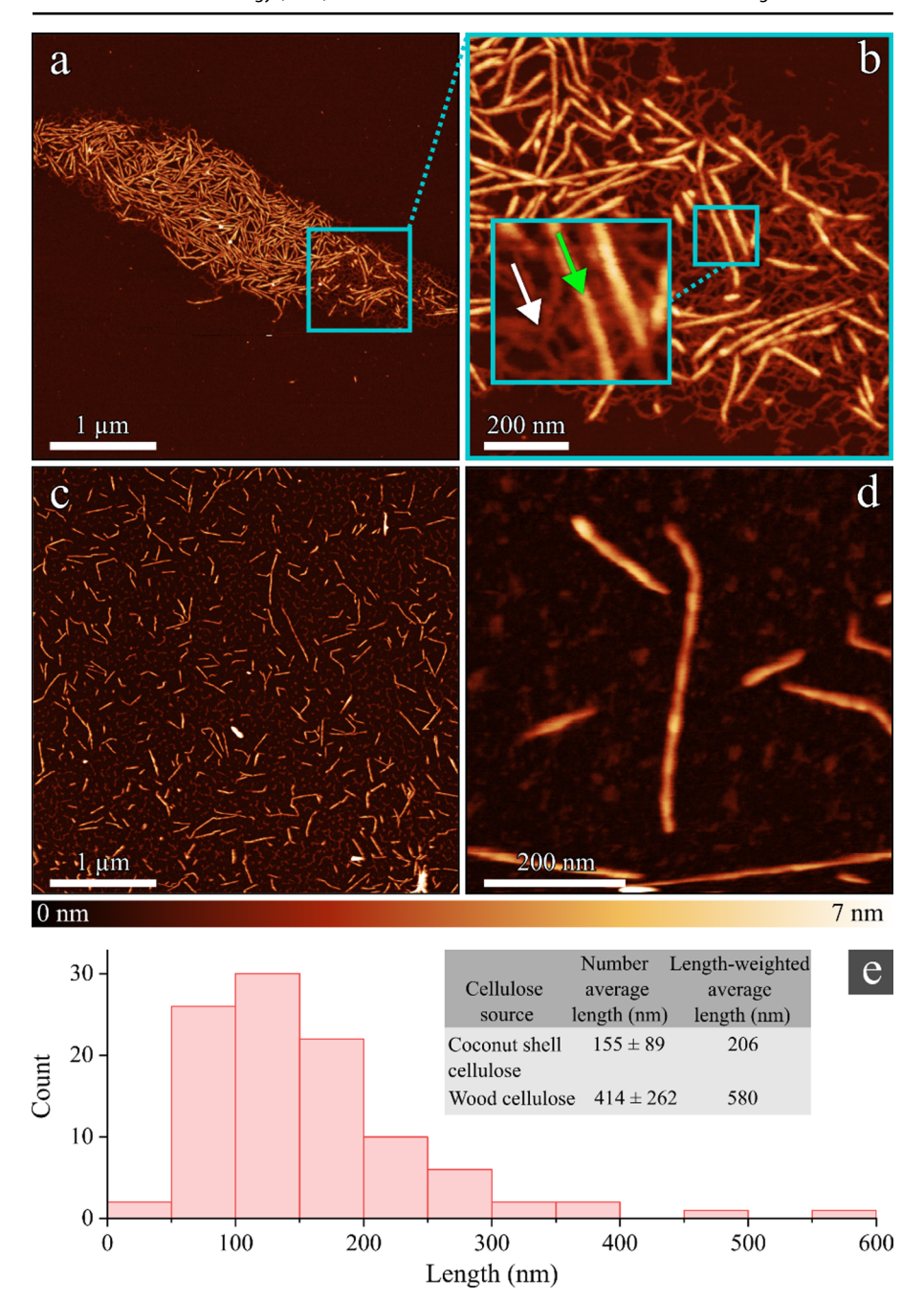


Fig. 3 a Group of TOCCNFs after tip sonication for 40 min, **b** smaller scan size topography map of the same group of TOCCNFs in **a**, inset: close-up of amorphous cellulose (white arrow) and crystal-line cellulose (green arrow), **c** topography map of TOCCNFs after 80 min of tip sonication, **d** close-up topography map of individual TOCCNF, **e** length distribution histogram for TOCCNFs and table comparison to wood CNFs from same method of preparation (Shinoda et al. 2012)

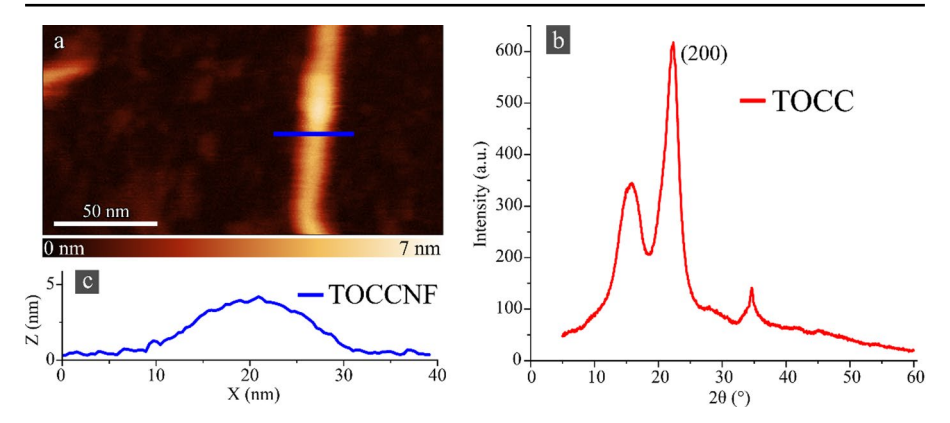


Fig. 4 a High resolution non-contact AFM image of a TEMPO-oxidized coconut cellulose nanofibril (TOCCNF), **b** diffractogram of TEMPO-oxidized coconut cellulose (TOCC), **c** a line profile of the AFM image displaying the fibril's width and height

Fig. 4a). In contrast to the other AFM scans, the lateral piezo transducers were operated open-loop for these high-magnification scans to reduce noise introduced by the position sensors and improve instrumental accuracy.

We then carried out X-ray diffraction (XRD) on TEMPO-oxidized coconut cellulose (TOCC) and used the Debye-Scherrer method to determine the nanofibril width and found it to be 6.63 nm (diffractogram presented in Fig. 4b). To compare this value with the horizontal profiles taken from the non-contact AM-AFM images (representative profile shown in Fig. 4a), we need to take into account the AFM tip radius used for this scan, approximately 8 nm. This approximately contributes an additional 16 nm (8 nm on each side) to the measured width, resulting in a profile base width of around 22 nm (Fig. 4c). After accounting for the tip-induced distortion, the true width of the cellulose nanofibril is estimated to be 6 nm, which is close to the 6.63 nm value derived from the Debye-Scherrer method. The height signal given from these measurements is around 3.5 nm, which is lower than the calculated width but expected if the fibril shape is uniform in height and width. At these low heights, the tip is still in range of the attractive van der Waals force region of the substrate, leading to an underestimation of the true nanofibril height (Santos et al. 2011). This close agreement between these two complementary methods indicates that the Debye-Scherrer method and high-resolution AFM profiling are viable procedures for nanoscale width estimation. The AFM profiles were taken on individual nanofibrils, whereas the X-ray diffractogram represents an average width of many nanofibrils.

Using the Segal method, we then determined a crystallinity index of 67% based on the diffractogram in Fig. 4b. This is slightly lower than the 71% seen from softwoods (Douglas fir), but similar to the 66.1% and 68.2% seen from potato tuber and rice straw respectively (Abe and Yano 2009). This could be in part due to the morphology of the coconut itself, its curvedness allowing for less crystalline regions as those regions tend to be straight.

To determine the weight% of the three major components — cellulose, hemicellulose, and lignin — dried weight measurements were taken after each chemical pretreatment step (Wang et al. 2021). The lignocellulosic biomass by weight was



32.1% cellulose, 39.6% hemicellulose, and 28.3% lignin. When compared to bamboo (47.2% cellulose, 23.9% hemicellulose, and 25.3% lignin) and Douglas fir (45.18% cellulose, 18.62% hemicellulose, and 25.01% lignin), there is ~14% less cellulose and ~18% more hemicellulose in the coconut (Bai et al. 2013; Zhu and Yadama 2016). Lignin content is also $\sim 3\%$ higher in the coconut, which, in combination with the increased hemicellulose percentage, could explain the extraordinary toughness seen in the coconut. The coconut is a composite material; the lignin and hemicellulose effectively act as a matrix, with the cellulose fibrils being the filler. In this case, the composite material has benefitted from an increased matrix percentage, holding the filler together more optimally to allow for higher distribution of stresses, resulting in an increase in toughness (Gordon 1980; Hulugappa et al. 2016). This is especially true due to the strong interfacial forces between hemicellulose and cellulose formed through hydrogen bonding (Mazumder and Zhang 2023). These cellulose fibrils are bonded to the matrix well enough to not only allow for an increase in toughness but also to maintain an impressive compressive strength of ~253 MPa (Flores-Johnson et al. 2018). The Douglas fir, with less matrix and more filler, has lower toughness and is therefore more brittle than the coconut. The Douglas fir also features an elastic modulus of 13.4 GPa, higher than the 8-10 GPa of the coconut (Senalik and Farber 2021). However, this higher elastic modulus does not translate into a stronger material in the Douglas fir, as its compressive strength is 5 times less than that of the coconut, ~50 MPa (Senalik and Farber 2021). Arguably, these properties reflect different requirements the lignocellulosic material needs to meet in each of the two species. A tree requires more stiffness to reduce swaying, whereas the coconut needs to withstand falls from great heights onto hard surfaces without cracking to maintain its chances to germinate.

Ultimately, the coconut is an exceptionally high-performing material, particularly notable for its impressive toughness. While this can be attributed to hierarchical structures at larger length scales, our findings reveal those aren't the only contributing factors. We have identified nanoscale structural differences between coconut and wood, providing a deeper insight that the enhanced mechanical performance of the coconut may already be present at the nanoscale. This discovery not only highlights the intricate and sophisticated nature of coconut endocarp's internal structure but also offers valuable insights into the potential design principles of high-performing lignocellulosic materials. This presents an exciting opportunity, providing a unique blueprint for the development and optimization of materials with exceptional mechanical properties starting at the nanoscale. The implications of this work extend beyond coconuts, offering a pathway for the development of sustainable and high-performance materials inspired by the natural world.

Conclusion

In conclusion, this study of the coconut endocarp has revealed new aspects of its molecular composition and structure at the nano- and microscales. Through a series of chemical treatments and exfoliation techniques, we have discovered the entangled structure of the strongly elongated sclereid cells, revealing that this material actu-



ally utilizes high-aspect ratio structural elements on two separate length scales — the other one being the cellulose nanofibrils, which we have successfully isolated and characterized. These nanofibrils have a distinct morphology, a relatively shorter length of around 155 ± 89 nm and a width of around 6 nm, as well as a crystallinity of around 67%. We also found that these nanofibrils are surrounded by more lignin, comprising 28.3% of the biomass, and by significantly more hemicellulose (39.6% of the biomass), compared to wood. This increase in matrix, in combination with a shorter length of crystalline cellulose nanofibrils, proves to be the blueprint for one of the toughest lignocellulosic biomaterials.

These findings provided new insights into the origins of the unique mechanical properties of this abundant lignocellulosic biomass. Optimizing material design based on the unique properties and structures of the coconut could enable the development of lightweight, high-strength protective gear offering superior impact resistance. Ultimately, this research not only paves the way for innovative applications of coconut-derived materials but also contributes to the broader field of materials science by providing insights into how fibril dimension and hierarchical structure can enhance mechanical performance.

Author contributions Conceptualization was done by HCS. Methodology was done by JS. Validation was done by HCS. Formal analysis was done by JS. Investigation was done by JS, and JS wrote the original draft. JS and HCS reviewed and edited the manuscript. Visualization was done by JS and HCS. Supervision and funding acquisition were done by HCS.

Funding This material is based upon work supported by the National Science Foundation under Award Nos. DMR-1905902, and DMR-2105158.

Data availability The data that support the findings of this study are openly available in the Harvard Dataverse at https://doi.org/10.7910/DVN/CVVZKE).

Declarations

Conflict of interest The authors declare no competing interests.

Open Access This article is licensed under a Creative Commons Attribution 4.0 International License, which permits use, sharing, adaptation, distribution and reproduction in any medium or format, as long as you give appropriate credit to the original author(s) and the source, provide a link to the Creative Commons licence, and indicate if changes were made. The images or other third party material in this article are included in the article's Creative Commons licence, unless indicated otherwise in a credit line to the material. If material is not included in the article's Creative Commons licence and your intended use is not permitted by statutory regulation or exceeds the permitted use, you will need to obtain permission directly from the copyright holder. To view a copy of this licence, visit http://creativecommons.org/licenses/by/4.0/.

References

Abe K, Yano H (2009) Comparison of the characteristics of cellulose microfibril aggregates of wood, rice straw and potato tuber. Cellulose 16:1017–1023. https://doi.org/10.1007/s10570-009-9334-9



Bai Y-Y, Xiao L-P, Shi Z-J, Sun R-C (2013) Structural variation of bamboo lignin before and after ethanol organosolv pretreatment. Int J Mol Sci 14:21394–21413. https://doi.org/10.3390/ijms141121394

Besbes I, Alila S, Boufi S (2011) Nanofibrillated cellulose from TEMPO-oxidized eucalyptus fibres: effect of the carboxyl content. Carbohydr Polym 84:975–983. https://doi.org/10.1016/j.carbpol.2010.12.0 52

Borrega M, Gibson LJ (2015) Mechanics of balsa (Ochroma pyramidale) wood. Mech Mater 84:75–90. h ttps://doi.org/10.1016/j.mechmat.2015.01.014

da Silva Perez D, Montanari S, Vignon MR (2003) TEMPO-mediated oxidation of cellulose III. Biomacromolecules 4:1417–1425. https://doi.org/10.1021/bm034144s

Daicho K, Saito T, Fujisawa S, Isogai A (2018) The crystallinity of nanocellulose: dispersion-induced disordering of the grain boundary in biologically structured cellulose. ACS Appl Nano Mater 1(10):5774–5785. https://doi.org/10.1021/acsanm.8b01438

de Nooy AEJ, Besemer AC, van Bekkum H (1995) Highly selective nitroxyl radical-mediated oxidation of primary alcohol groups in water-soluble glucans. Carbohydr Res 269:89–98. https://doi.org/10.1016/0008-6215(94)00343-e

Dixon PG, Gibson LJ (2014) The structure and mechanics of Moso bamboo material. J R Soc Interface 11:20140321. https://doi.org/10.1098/rsif.2014.0321

Eichhorn SJ, Hughes M, Snell R, Mott L (2000) Strain induced shifts in the raman spectra of natural cellulose fibers. J Mater Sci Lett 19:721–723. https://doi.org/10.1023/a:1006787300815

Elazzouzi-Hafraoui S, Nishiyama Y, Putaux J-L et al (2007) The shape and size distribution of crystalline nanoparticles prepared by acid hydrolysis of native cellulose. Biomacromolecules 9:57–65. https://doi.org/10.1021/bm700769p

Fan F, Zhu M, Fang K et al (2021) Extraction and characterization of cellulose nanowhiskers from TEMPO oxidized sisal fibers. Cellulose 29:213–222. https://doi.org/10.1007/s10570-021-04305-8

Flores-Johnson EA, Carrillo JG, Zhai C et al (2018) Microstructure and mechanical properties of hard *Acrocomia mexicana* fruit shell. Sci Rep. https://doi.org/10.1038/s41598-018-27282-8

French AD, Santiago Cintrón M (2013) Cellulose polymorphy, crystallite size, and the Segal crystallinity index. Cellulose 20:583–588. https://doi.org/10.1007/s10570-012-9833-y

Gibson LJ (2012) The hierarchical structure and mechanics of plant materials. J R Soc Interface 9:2749–2766. https://doi.org/10.1098/rsif.2012.0341

Gludovatz B, Walsh F, Zimmermann EA et al (2017) Multiscale structure and damage tolerance of coconut shells. J Mech Behav Biomed Mater 76:76–84. https://doi.org/10.1016/j.jmbbm.2017.05.024

Gordon (1980) Composites with high work of fracture. Philos Trans R Soc Lond Ser A Math Phys Sci 294:545–550. https://doi.org/10.1098/rsta.1980.0063

Habibi Y, Chanzy H, Vignon MR (2006) TEMPO-mediated surface oxidation of cellulose whiskers. Cellulose 13:679–687. https://doi.org/10.1007/s10570-006-9075-y

Hubbell CA, Ragauskas AJ (2010) Effect of acid-chlorite delignification on cellulose degree of polymerization. Bioresour Technol 101:7410–7415. https://doi.org/10.1016/j.biortech.2010.04.029

Hulugappa B, Achutha MV, Suresha B (2016) Effect of fillers on mechanical properties and fracture toughness of glass fabric reinforced epoxy composites. J Miner Mater Charact Eng 04:1–14. https://doi.org/10.4236/jmmce.2016.41001

Isogai A, Saito T, Fukuzumi H (2011) TEMPO-oxidized cellulose nanofibers. Nanoscale 3:71–85. https://doi.org/10.1039/c0nr00583e

Isogai T, Saito T, Isogai A (2010) Wood cellulose nanofibrils prepared by TEMPO electro-mediated oxidation. Cellulose 18:421–431. https://doi.org/10.1007/s10570-010-9484-9

Jakob M, Mahendran AR, Gindl-Altmutter W et al (2022) The strength and stiffness of oriented wood and cellulose-fibre materials: a review. Prog Mater Sci 125:100916. https://doi.org/10.1016/j.pmatsci.2 021.100916

Kaffashsaie E, Yousefi H, Nishino T et al (2021) Direct conversion of raw wood to TEMPO-oxidized cellulose nanofibers. Carbohydr Polym 262:117938. https://doi.org/10.1016/j.carbpol.2021.117938

Lauer C, Schmier S, Speck T, Nickel KG (2018) Strength-size relationships in two porous biological materials. Acta Biomater 77:322–332. https://doi.org/10.1016/j.actbio.2018.07.010

Ma P, Fu S, Zhai H et al (2012) Influence of TEMPO-mediated oxidation on the lignin of thermomechanical pulp. Bioresour Technol 118:607–610. https://doi.org/10.1016/j.biortech.2012.05.037

Mazumder S, Zhang N (2023) Cellulose–Hemicellulose–Lignin interaction in the secondary cell wall of coconut endocarp. Biomimetics 8:188. https://doi.org/10.3390/biomimetics8020188



- Modenbach, Nokes (2014) Effects of Sodium Hydroxide Pretreatment on Structural Components of Biomass. Transactions of the ASABE 1187–1198. https://doi.org/10.13031/trans.57.10046
- Perera D, Li L, Walsh C et al (2023) Natural spider silk nanofibrils produced by assembling molecules or disassembling fibers. Acta Biomater 168:323–332. https://doi.org/10.1016/j.actbio.2023.06.044
- Popescu, Tibirna, Raschip, et al (2008) Bulk and surface characterization of unbleached and bleached softwood kraft pulp fibres. Cellulose Chemistry and Technology 42:525–547
- Saito T, Isogai A (2004) TEMPO-mediated oxidation of native cellulose. The effect of oxidation conditions on chemical and crystal structures of the water-insoluble fractions. Biomacromolecules 5:1983–1989. https://doi.org/10.1021/bm0497769
- Salvini VR, Pandolfelli VC, Spinelli D (2018) Mechanical Properties of Porous Ceramics. Recent Advances in Porous Ceramics 171–199. https://doi.org/10.5772/intechopen.71612
- Santos S, Barcons V, Christenson HK et al (2011) The intrinsic resolution limit in the atomic force microscope: implications for heights of nano-scale features. PLoS One 6(8):e23821. https://doi.org/10.1371/journal.pone.0023821
- Scheller HV, Ulvskov P (2010) Hemicelluloses. Annu Rev Plant Biol 61:263–289. https://doi.org/10.1146/annurev-arplant-042809-112315
- Schmier S, Hosoda N, Speck T (2020) Hierarchical structure of the Cocos nucifera (coconut) endocarp: functional morphology and its influence on fracture toughness. Molecules 25:223. https://doi.org/10.3390/molecules25010223
- Segal L, Creely JJ, Martin AE, Conrad CM (1959) An empirical method for estimating the degree of crystallinity of native cellulose using the X-ray diffractometer. Text Res J 29:786–794. https://doi.org/10.1177/004051755902901003
- Senalik CA, Farber B (2021) Mechanical properties of wood. In: Wood handbook—wood as an engineering material. General Technical Report FPL-GTR-282. U.S. Department of Agriculture, Wisconsin, pp 1–46
- Shinoda R, Saito T, Okita Y, Isogai A (2012) Relationship between length and degree of polymerization of TEMPO-oxidized cellulose nanofibrils. Biomacromolecules 13:842–849. https://doi.org/10.1021/bm2017542
- Silliman J, Koebley SR, Schniepp HC (2024) The cribellate nanofibrils of the Southern house spider: extremely thin natural silks with outstanding extensibility. Adv Funct Mater. https://doi.org/10.100 2/adfm.202408409
- Tashiro K, Kobayashi M (1991) Theoretical evaluation of three-dimensional elastic constants of native and regenerated celluloses: role of hydrogen bonds. Polymer 32:1516–1526. https://doi.org/10.1016/0032-3861(91)90435-1
- Wang Y, Yang Y, Qu Y, Zhang J (2021) Selective removal of lignin with sodium chlorite to improve the quality and antioxidant activity of xylo-oligosaccharides from lignocellulosic biomass. Bioresour Technol 337:125506. https://doi.org/10.1016/j.biortech.2021.125506
- Yan J, Taskonak B, Platt JA, Mecholsky JJ (2008) Evaluation of fracture toughness of human dentin using elastic–plastic fracture mechanics. J Biomech 41:1253–1259. https://doi.org/10.1016/j.jbiomech.20 08.01.015
- Yi T, Zhao H, Mo Q et al (2020) From cellulose to cellulose nanofibrils—a comprehensive review of the preparation and modification of cellulose nanofibrils. Materials 13:5062. https://doi.org/10.3390/ma13225062
- Zhang K, Barhoum A, Xiaoqing C, et al (2018) Cellulose Nanofibers: Fabrication and Surface Functionalization Techniques. In: Handbook of Nanofibers. Springer International Publishing, pp 1–41
- Zhu R, Yadama V (2016) Effects of hot water extraction pretreatment on physicochemical changes of Douglas fir. Biomass Bioenerg 90:78–89. https://doi.org/10.1016/j.biombioe.2016.03.028

Publisher's Note Springer Nature remains neutral with regard to jurisdictional claims in published maps and institutional affiliations.

